Nonequilibrium molecular dynamics simulation of free-molecule gas flows in complex geometries with application to Brownian motion of aggregate aerosols

Michael H. Peters*

Department of Chemical Engineering, Florida State University and Florida A&M University, Florida Agricultural and Mechanical University/Florida State University College of Engineering, Tallahassee, Florida 32316-2175

(Received 31 March 1994; revised manuscript received 8 August 1994)

A nonequilibrium molecular dynamics method is presented for the study of free-molecule, rarefied gas flows in complex geometries. Simulation results for a system of N rigid spheres in a rarefied gas are given, including particle friction tensor and force autocorrelation function. For single spheres, simulation results are shown to agree with known analytical results. For a two-sphere system, computational results are presented that indicate the two-sphere friction tensor is nonsymmetric, as opposed to the symmetric behavior in continuum and near continuum fluids. The nonsymmetric behavior can be traced to geometric shielding effects and leads to an effective attractive force between two spheres in free-molecule flows. It is possible to use the nonequilibrium molecular dynamics method given here to determine the many-sphere friction behavior for combined use in Langevin dynamics. Such a procedure, in principle, could allow for a rigorous, long-term dynamical analysis of particles in complex fluid systems.

PACS number(s): 05.20.Dd, 02.70.Ns

I. INTRODUCTION

In many practical problems involving the dynamic interactions of gases with surfaces, the gas flow in the vicinity of the surface is so rarefied that the intermolecular gas interactions can be neglected. This regime, known as the "free-molecule" regime in gas dynamics, is quantified by a large, local Knudsen number ($N_{\mathrm{Kn}} \gg 1$), where the Knudsen number represents the ratio of the mean free path of the gas to a characteristic length scale of the system, e.g., the characteristic length of an object immersed in the gas flow. Practical systems where such flows exist include the Brownian motion of aggregate aerosols in rarefied gases, the dynamics of space vehicles in rarefied planetary atmospheres, gas dynamic interactions of particles and walls, and the flow of gases in catalytic pores and membranes, among others. Despite the simpler molecular nature of rarefied gas flows, these "practical" systems are characterized by complex geometries making analytical solutions extremely difficult. Fortunately, as will be shown here, molecular dynamics methods for nonequilibrium systems can be developed to numerically evaluate all types of rarefied gas flows in complex geometries, including such complex issues as the Brownian dynamics of arbitrarily shaped particles.

Specifically, the nonequilibrium molecular dynamics technique used in this study has been called the natural nonequilibrium molecular dynamics (NNMD) method [1]. In this technique, the boundary conditions and/or initial conditions are included in the simulation as they actually or "naturally" occur in the physical experiment [2]. A significant concern for the use of NNMD is the possibility of a large spatial system dimension and, hence, a large number of molecules necessary for simulation studies. Despite the necessarily large system size, however, NNMD has been applied to a number of flow systems, including Couette flow and flows over simple objects, such as flat planes and cylinders [3,4].

In the case of free-molecule flows, it is shown here that a computationally simple NNMD scheme can be constructed that allows for a comprehensive analysis of rarefied gas flows in highly complex geometries. The simplifications are associated with the free-molecule assumption that reflected molecules from object surfaces do not affect the distribution of incoming molecules from a given source [5]. It is to be noted that Chan and Dahneke [6] have previously addressed this problem using what they called a type of "direct simulation Monte Carlo method" [7]. Their (Monte Carlo) method was based on ensemble averaging of allowed or possible collisions with small geometric segments of the surfaces by the self-collisionless gas molecules and was used to predict the steady-state gas frictional forces acting on a chain of spheres. As will be shown here, the current molecular dynamics method is more general and, for example, can take into account important time dependent phenomena, such as memory dependent friction, Brownian motion, and force autocorrelation functions. The NNMD method also readily allows for all types of complex geometries and gas-surface interactions, as well as being readily extended to include gas intermolecular interactions. We also note that the force autocorrelation functions for Brownian particles of arbitrary shape (obtainable here) are particularly important for the resolution of generalized Langevin equations and subsequent use in applications, as discussed in more detail below.

We begin with a presentation of the computational technique followed by a comparison of the results to known analytical solutions for problems involving particle dynamics in rarefied gas flows. Finally, some alterna-

*Electronic address: Peters@scri.fsu.edu

tive results are presented for complex particle geometries not accessible analytically.

II. FREE-MOLECULE MOLECULAR DYNAMIC SIMULATIONS

In the NNMD method, the nonequilibrium system is usually connected to equilibrium reservoirs. For example, in Poiseuille flow the inlet fluid to the tube comes from an equilibrium reservoir maintained at some fixed temperature and pressure or density. Similarly, the fluid exits to another equilibrium reservoir maintained at different conditions. The equilibrium reservoirs (isothermal, isoenergetic, isobaric, etc.) can be generated by well-known equilibrium molecular dynamics methods (see, e.g., [8] or [9]). The interactions of the fluid molecules with vessel walls can be treated using simple specular or diffuse reflection conditions, or more exactly by considering the fluid molecule interactions with the wall molecules.

A problem of specific interest here is the relative motion of a fluid over objects of complex shapes, such as aggregate aerosols. In this problem, equilibrium conditions persist at distances far from the object. Therefore, it is necessary to surround the objects with an equilibrium reservoir maintained, for example, at a fixed temperature and number density (canonical equilibrium ensemble). The nonequilibrium system contained within the reservoirs will be called the control volume (CV) in this study. Generally speaking, for unbounded systems, it is not known *a priori* exactly how far from the object to fix the position of the equilibrium reservoirs. For example, in low-Reynolds-number flow over a sphere, it is well known that the equilibrium conditions occur at distances some eight to ten sphere diameters from the sphere center [10]. However, since we are presumably interested in problems where analytical solutions are difficult to obtain or not known, the decay length to an equilibrium state is generally an unknown quantity. The position of the reservoirs, must, therefore, be determined by trial and error, i.e., moving the reservoir outward until no changes in macroscopic variables (as averages over molecular properties) are observed. In free-molecule flows, however, not only can collisions between the molecules be neglected in the CV, but also the reflected molecules from the surface are assumed not to affect the incoming molecules from the reservoirs. As shown below, a rather simple nonequilibrium molecular dynamic simulation can be constructed for this practically important case.

For free-molecule flows, a cubical control volume with side lengths l_0 is selected to surround the object but lie within a standard equilibrium cell (e cell) common to equilibrium molecular dynamics simulations as shown in Fig. 1. The side lengths of the equilibrium cell are denoted by l_e with number density and temperature denoted as n_∞ and T_∞, respectively. Molecules that enter the control volume from the equilibrium cell are identified—these molecules are denoted as "active molecules." However, in order not to affect the "incoming" molecular distribution, in space and time, a "passive image" of the molecule moves freely throughout the control volume

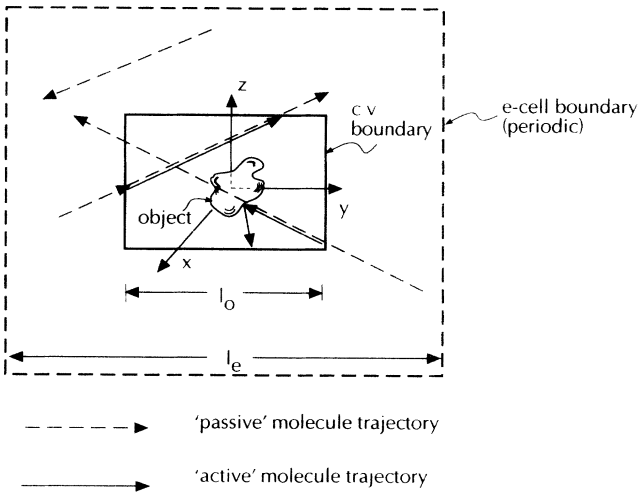

FIG. 1. Illustration of the molecular dynamics method for free-molecule flows over complex objects. Equilibrium-cell (e-cell) molecular trajectories are denoted by dashed lines; control volume molecular trajectories are denoted by solid lines. For free-molecule flows, the flux of molecules to surfaces follows an equilibrium Maxwellian distribution.

with its trajectory unaltered, except perhaps by collisions with other passive molecules, as shown in Fig. 1. This ensures that all molecules that arrive from infinity to the surface of the object are Maxwellian distributed molecules. The equilibrium cell molecules are subject to the usual periodic boundary conditions along the sides of the cell, as well as to intermolecular interactions. Alternatively, the control volume could be surrounded by replicated, equilibrium cells reducing the total number of intermolecular interaction calculations required in the equilibrium cell. In any case, within the control volume the gas flow is assumed to be rarefied and intermolecular interactions among "active" molecules can be neglected.

Generally, n_∞ and T_∞ are in the range such that the free-molecule flow criteria, $\lambda \gg d_{\max}$ is satisfied, where $\lambda = \lambda(n_\infty, T_\infty)$ is the mean free path of the gas and $d_{\max}$ is the maximum length scale of the object. The equilibrium cell dimension, l_e must be greater than λ in order to have a statistically meaningful equilibrium ensemble. As shown in the numerical examples below, for gas flows around submicron particles at standard conditions this generally results in a large number of molecules, N ($= n_\infty l_e^3$), in the equilibrium cell (typically 10^4 or higher).

At the start of the simulation, N molecules are generated in the equilibrium cell with a Maxwellian velocity distribution at temperature T_∞ and average velocity in direction l denoted by v_l (see, e.g., [11]). Corrections to the sampled velocity distribution are then invoked to ensure the correct temperature and average velocity (see Appendix). Molecules that initially lie in the CV, but not within the object, are the first "active" molecules.

The determination of molecular trajectories and collisions with surfaces in the CV or their escape from the CV can be carried out in a variety of ways. Here, we use the so-called time table method [12], which is adapted to

the gas dynamic problem as follows.

First, it is determined whether or not molecules within the control volume will follow a trajectory that intersects with the surfaces present. For example, if the surfaces represent an aggregate aerosol comprised of spherical subunits, a "hard" collision of a molecule with any one of the spheres will possibly take place if

$$b_{ij} \leq \frac{(\sigma_i + d_j)}{2} , \tag{1}$$

where σ_i is the diameter of the ith molecule, d_j is the diameter of the jth sphere of the aggregate, and b_{ij} is computed as

$$b_{ij}^2 = r_{ij}^2 - \left[\mathbf{r}_{ij} \cdot \frac{\mathbf{v}_{ij}}{v_{ij}} \right]^2 . \tag{2}$$

In the last equation, $\mathbf{r}_{ij} \equiv \mathbf{r}_i - \mathbf{r}_j$ is the separation vector between the molecule (i) and the sphere (j) and $\mathbf{v}_{ij} = \mathbf{v}_i - \mathbf{v}_j$ is the relative velocity ($v_{ij} \equiv |\mathbf{v}_{ij}|$). Furthermore, the time for the contact between the molecule and sphere for a "hard" collision is easily determined as

$$t_{ij} = \frac{1}{v_{ij}} \left\{ - \frac{(\mathbf{r}_{ij} \cdot \mathbf{v}_{ij})}{v_{ij}} - \left[\left[\frac{(\sigma_i + d_j)}{2} \right]^2 - b_{ij}^2 \right]^{1/2} \right\} . \tag{3}$$

We note that by "hard" collision, we are not taking into account the detailed gas-molecule-surface molecule interactions. However, the method could easily be modified to do so by expanding the diameter of the sphere outward to encompass the interaction force range (see, e.g., [13] for MD with continuous interaction potentials). The relatively short-time "soft" collision could then be determined in a separate routine. Complicated features such as surface roughness, molecular condensation, among others, could also be treated by this method. For central force interactions, effective hard-sphere diameters can be used (see, e.g., [14]). For a "specular" collision of a spherical molecule and a spherical subunit the velocity change is simply given by

$$\Delta \mathbf{v}_i = \frac{-2M_j (\mathbf{v}_{ij} \cdot \mathbf{r}_{ij}) \mathbf{r}_{ij}}{[\frac{1}{2}(\sigma_i + d_j)]^2} \tag{4}$$

and

$$\Delta \mathbf{v}_j = \frac{+2M_i (\mathbf{v}_{ij} \cdot \mathbf{r}_{ij}) \mathbf{r}_{ij}}{[\frac{1}{2}(\sigma_i + d_j)]^2} , \tag{5}$$

where the reduced masses are defined as

$$M_j = \frac{m_j}{(m_i + m_j)} , \tag{6}$$

$$M_i = \frac{m_i}{(m_i + m_j)} , \tag{7}$$

and the post-collisional velocities are given as

$$\mathbf{v}_i' = \mathbf{v}_i + \Delta \mathbf{v}_i , \tag{8}$$

$$\mathbf{v}_j' = \mathbf{v}_j + \Delta \mathbf{v}_j , \tag{9}$$

Also, note that $\mathbf{r}_{ij}$ in the above formulas is the separation distance vector at the point of contact. For "diffuse" reflection, on the other hand, the post-collisional molecular velocities, $\mathbf{v}_i'$, are selected from the following probability distribution for an impinging molecule of velocity $\mathbf{v}_i$ to be reemitted with a velocity $\mathbf{v}_i'$ [5],

$$R(\mathbf{v}_i \rightarrow \mathbf{v}_i') = |(\mathbf{v}_i' - \mathbf{v}_j) \cdot \mathbf{n}_j| \frac{1}{(2\pi k T_j / m_i)} \times \exp \left\{ \frac{m_i |\mathbf{v}_i' - \mathbf{v}_j|^2}{2kT_j} \right\} . \tag{10}$$

T_j is the surface temperature of the jth spherical subunit and $\mathbf{n}_j$ is a unit vector normal to the sphere (j) surface, viz., $\mathbf{n}_j \equiv \mathbf{r}_{ij} / |\mathbf{r}_{ij}|$. For a spherical coordinate system at the center of sphere j (or local Cartesian coordinate system at the surface of sphere j), we have

$$R \equiv R_r(v_{ri} \rightarrow v_{ri}') R_\theta(v_{\theta i} \rightarrow v_{\theta i}') R_\phi(v_{\phi i} \rightarrow v_{\phi i}') , \tag{11}$$

where

$$R_r = \left[\frac{kT_w}{m} \right] |(v_{r_i}' - v_{r_j})| \exp \left[- \frac{m_i (v_{r_i}' - v_{r_j})^2}{2kT_w} \right] , \tag{12}$$

$$R_\theta = \left[\frac{2\pi k T_w}{m} \right]^{1/2} \exp \left[- \frac{m_i (v_{\theta_i}' - v_{\theta_j})^2}{2kT_w} \right] , \tag{13}$$

$$R_\phi = \left[\frac{2\pi k T_w}{m} \right]^{1/2} \exp \left[- \frac{m_i (v_{\phi_i}' - v_{\phi_j})^2}{2kT_w} \right] . \tag{14}$$

Thus, R_θ and R_ϕ represent normal distributions with variance $(2kT_w/m)^{-1/2}$ and mean values v_{θ_j} and v_{ϕ_j}, respectively. R_r may be sampled following Ref. [7] [see Eq. (7.9) therein].

Once sampled the velocity components in the spherical coordinate system are converted to rectangular components, viz.,

$$v_{i_x}' = \sin\theta \cos\phi v_{i_r}' + \cos\theta \cos\phi v_{i_\theta}' - \sin\phi v_{i_\phi}' , \tag{15}$$

$$v_{i_y}' = \sin\theta \sin\phi v_{i_r}' + \cos\theta \sin\phi v_{i_\theta}' + \cos\phi v_{i_\phi}' , \tag{16}$$

$$v_{i_z}' = \cos\theta v_{i_r}' - \sin\theta v_{i_\theta}' , \tag{17}$$

where

$$\cos\theta = \frac{z_i - z_j}{r_{ij}} , \tag{18}$$

$$\sin\theta = \frac{[(x_i - x_j)^2 + (y_i - y_j)^2]^{1/2}}{r_{ij}} , \tag{19}$$

$$\cos\phi = \frac{(x_i - x_j)}{[(x_i - x_j)^2 + (y_i - y_j)^2]^{1/2}} , \tag{20}$$

and

$$\sin\phi = \frac{(y_i - y_j)}{[(x_i - x_j)^2 + (y_i - y_j)^2]^{1/2}} , \tag{21}$$

The post-collisional surface velocity follows from momentum conservation. Of course, the above analysis simplifies considerably when the surfaces are held fixed ($\mathbf{v}_j = \mathbf{v}_j' = \mathbf{0}$) or they are so massive ($M_j \cong m_j$ and $M_i \cong 0$)

that their velocity change can be neglected ($\Delta \mathbf{v}_j \cong \mathbf{0}$).

Finally, we need to know the escape times of molecules in the CV whose trajectories will not intersect with surfaces and will, therefore, escape the CV. These are easily determined as [12]

$$t_i^k = \frac{\left[\frac{(l+\sigma_i)}{2}\left[\frac{\mathbf{v}_i \cdot \mathbf{e}_k}{|\mathbf{v}_i \cdot \mathbf{e}_k|}\right] - \mathbf{e}_k \cdot \mathbf{r}_i\right]}{\mathbf{e}_k \cdot \mathbf{v}_i} , \tag{22}$$

where $\mathbf{e}_k$ is a unit vector in the space-fixed Cartesian frame (see Fig. 1).

An analysis similar to that of Eq. (3) must also be carried out for collisions between the "passive" molecules of the equilibrium cell. This will also lead to the corresponding time denoted by t_{mn}^e, where the equilibrium-cell molecule interactions are treated as effective hard-sphere collisions for the sake of simplicity.

Now, the timetable method is a variable time step method where the time step of the simulation, Δt, is selected as the minimum time, i.e.,

$$\Delta t = \min(t_{ij}, t_i^k, t_{mn}^e) . \tag{23}$$

After selection of the time step, Δt, the molecules (passive and active) are then moved along straight line trajectories as

$$\Delta \mathbf{r}_i = \mathbf{v}_i \Delta t \tag{24}$$

and

$$\Delta \mathbf{r}_i^e = \mathbf{v}_i^e \Delta t , \tag{25}$$

where the superscript "e" denotes the equilibrium-cell molecules. For passive molecules that escape the equilibrium cell, periodic boundary conditions are applied. Also, for any passive molecule that enters the CV, an "active" molecule is created with that position and velocity. Thus, the flux of molecules into the CV is an equilibrium flux consistent with the boundary conditions of the problem. Over the time step, Δt, if an active molecule collides with a surface, new velocities are assigned and the momentum changes are recorded. If an active molecule escapes the CV, it is eliminated from the simulation (lost to the infinitely large reservoir). Thus, the molecular number density in the CV fluctuates somewhat with time about an average value, as expected for this open, nonequilibrium system. Of course, the molecular number density remains constant in the equilibrium cell. Note again the satisfaction of the free-molecule criteria of always maintaining a Maxwellian distribution of incoming molecules (with a certain number density, temperature, and average velocity) and that active molecules should not alter this distribution. Figure 2 gives a more specific breakdown of the simulation procedure.

An important aspect of rarefied gas flows in complex geometries is the phenomena of "shielding" and multiple reflection of gas molecules off object surfaces, which is

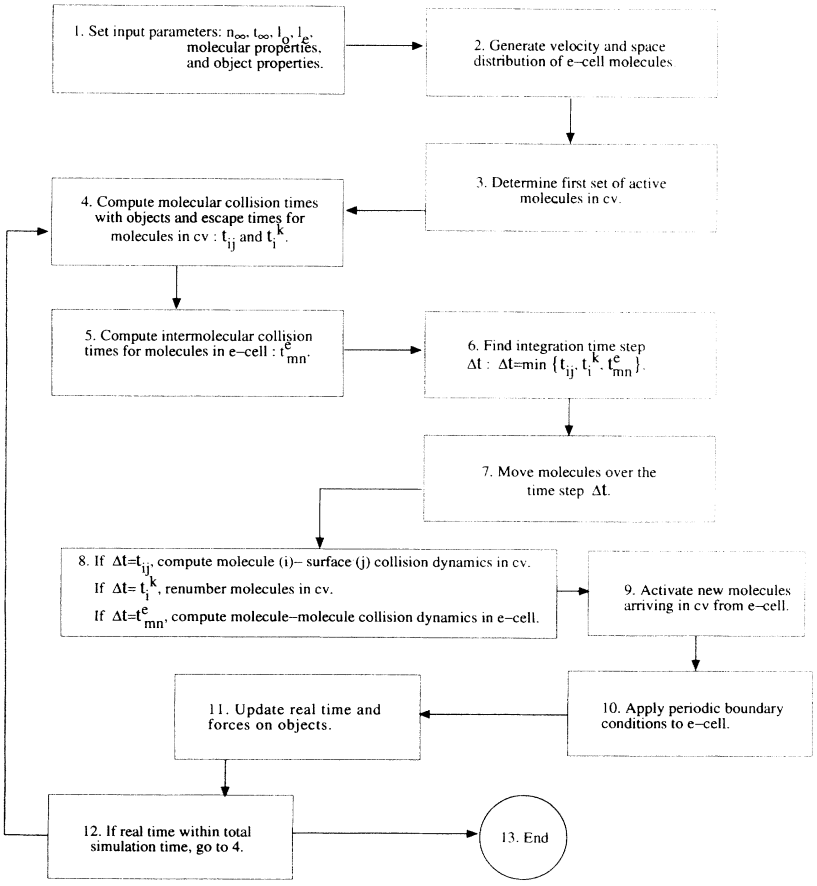

FIG. 2. Nonequilibrium molecular dynamics simulation procedures using the timetable method. The time steps are associated with intermolecular collisions in the equilibrium cell, collisions of active molecules with surfaces in the control volume (CV), and escape of active molecules from the CV.

implicitly included in the present approach. For concave objects, or complex surfaces, the active molecule may strike other surfaces upon reflection, and the entire molecular trajectory is followed in time until escape.

III. FORCES ON OBJECTS: FRICTION, DIFFUSION, AND FORCE AUTOCORRELATION

For hard collisions, the forces acting on the objects consist of a series of impulses due to colliding molecules. The time-average force acting on the object in any direction can be obtained by summing the momentum changes from molecule-surface collisions as

$$\langle F_l \rangle = \lim_{t_f \to \infty} \frac{1}{t_f} \int_0^{t_f} F_l dt = \lim_{t_f \to \infty} \frac{1}{t_f} \int_0^{t_f} \sum_k J_{lk} \delta(t - t_k) dt = \lim_{t_f \to \infty} \frac{1}{t_f} \sum_k J_{lk} , \tag{26}$$

where J_{lk} is the impulse of change in momentum in direction l associated with the kth collision.

An equally important quantity is the force autocorrelation function defined as

$$R_{lm}(\tau) = \langle F_l(\tau) F_m(0) \rangle = \lim_{S \to \infty} \frac{1}{2S} \int_{-S}^{S} F_l(t+\tau) F_m(t) dt , \tag{27}$$

which for impulsive forces becomes

$$R_{lm}(\tau) = \langle F_l(\tau) F_m(0) \rangle = \lim_{S \to \infty} \frac{1}{2S} \sum_i \sum_j J_{l_i} J_{m_j} \delta[\tau - (t_i - t_j)] , \tag{28}$$

where J_{l_i} is the change in momentum in direction l associated with the ith collision at time t_i.

In generalized Langevin equation theory, the particle friction tensor (for $m_j \gg m_i$) is related to the force autocorrelation function as ([15–17], and the references therein)

$$\zeta(t) = \frac{1}{kT} \int_0^t \langle \mathbf{F}(t-t') \mathbf{F}(0) \rangle^{\text{eq}} dt' , \tag{29}$$

where $\langle \ \rangle^{\text{eq}}$ denotes an equilibrium average force acting on a particle held in a fixed position in the fluid. For impulsive forces, the particle friction tensor expression becomes

$$\zeta_{lm}(t) = \lim_{S \to \infty} \frac{1}{2S} \frac{1}{kT} \sum_i \sum_{\substack{j \\ j \le i}} J_{li} J_{mj} \quad \text{for } (t_i - t_j) \le t \tag{30}$$

In simulations, the period S is finite and the above formula is approximate, but in any case S should be much greater than t. The generalized Einstein relation allows the computation of the particle diffusion tensor, $\mathbf{D}$, from the friction tensor as

$$\mathbf{D} = kT \zeta^{-1} . \tag{31}$$

Importantly, the determination of the particle friction tensor through (short-time) molecular dynamics force autocorrelation function calculations allows the analysis of relatively longer time step Brownian dynamics via solutions to the generalized Langevin equations (see, e.g., [18]). Such a (two-time) procedure (molecular dynamics followed by Brownian dynamics), in principle, allows particle phenomena for large characteristic time scales to be rigorously determined. The computationally prohibitive problem of determining large time scale particle phenomena through molecular dynamics alone is recently illustrated in protein dynamics (see Fig. 5 of Ref. [19]). Long-time protein dynamics are currently inaccessible by molecular dynamics. Here, we advocate a two-step procedure using molecular dynamics followed by generalized Langevin equation theory. Indeed, the generalized Langevin equation itself has been obtained by the so-called multiple time scales method [20]. Below, we present some example calculations of NNMD for single-sphere and multisphere aggregate particles.

IV. SINGLE-SPHERE AND TWO-SPHERE RESULTS

The friction tensor and force autocorrelation function for single isolated rigid spheres were determined in order to compare to known analytical results and test the accuracy of the computations. In the first "experiment," the equilibrium-cell molecules were given a finite average velocity v_l in direction l with the friction coefficient defined according to

$$\langle F_l \rangle = \zeta v_l . \tag{32}$$

An analytical expression for ζ is, of course, well known and given by (see, e.g., [21])

$$\zeta_{\text{anal}} = \frac{\pi m n |v_l| a^2}{2} f(s) , \tag{33}$$

when n is the molecular number density, m is the mass of a single gas molecule, a is its radius, and $f(s)$ is given by

$$f(s) = \frac{1}{s^2} \left[\frac{4s^4 + 4s^2 + 1}{2s} \operatorname{erf}(s) + \frac{2s^2 + 1}{\sqrt{\pi}} e^{-s^2} \right] + \frac{2}{3} \frac{\sigma}{s} \sqrt{\pi} , \tag{34}$$

with $s = |v_l| / (2kT/m)^{1/2}$ and $\sigma = 1$ or 0 for diffuse or specular molecular reflection, respectively. The asymptotic limits are of practical use and are given by

$$f(s) \to 2 \quad \text{as } s \to \infty , \tag{35}$$

$$f(s) \cong \frac{1}{s} \frac{1}{\sqrt{\pi}} \left[\frac{16}{s} + \frac{2}{3} \sigma \pi \right] \quad \text{for } s \ll 1 . \tag{36}$$

Note that in writing Eq. (34) it is assumed that the momentum and energy accommodation coefficients are equal and that the sphere temperature and gas temperature are also equal (for more details, see, e.g., [21]).

A specific system was selected for comparison purposes as detailed in Table I. Because of the necessarily large number of molecules in the equilibrium cell (25 000) as discussed above, the velocity distribution obtained

TABLE I. Input Parameters.

n_∞	$=2.5\times10^{25}$ (number)/m^3
N	$=25\,000$
l_e	$=1.0\times10^{-7}$ m
l_0	$=2.0\times10^{-8}$ m
m	$=6.625\times10^{-26}$ kg
d	$=1.0\times10^{-8}$ m
$T_\infty = T_w$	$=2.93.15$ K
σ_i	$=0.0$ m
Total number of time steps	$=10^5$

through Gaussian sampling followed closely the true distribution function. Note that for a smaller sample, molecular collisions or interactions in the equilibrium cell serve to create a true Gaussian distribution over time in the equilibrium cell (see, e.g., [22] and [23]).

Also, for the standard gas conditions selected as shown in Table I, the intermolecular collisions or interactions in the equilibrium cell are so infrequent that the equilibrium-cell gas can be approximately taken as an ideal gas system neglecting interactions entirely; this, of course, greatly reduces the computational time required (N^2 steps for each time interval). Of course, for other gas conditions in the equilibrium cell this may not be possible. All calculations reported here assume that the equilibrium cell gas is ideal except as noted.

Figure 3 gives a comparison of NNMD results for the friction coefficient under specular reflective boundary conditions with the analytical solution for the parameters listed in Table I. The results are normalized with respect to the small asymptotic limit of $\zeta_{\text{anal}}(s \ll 1)$. As can be seen, excellent results are obtained from NNMD. Furthermore, the standard deviations in the NNMD calculations (not shown) were less than a couple of percent of the mean values (shown). The standard deviations are obtained by repeating the calculations several times for different values of the initial seeds for generating the molecular velocity and space distributions. Similar excellent comparison for diffuse molecular reflection were also obtained, as shown in Fig. 4. No significantly different

TABLE II. Force autocorrelation calculations of the friction tensor, $\zeta_{lm}(t)/\zeta_{\text{anal}}$. Mean values are given below; standard deviations were with 5% or better for the values given below.

$t=0.15\times10^{-10}$ s

$$\begin{vmatrix} 0.998 & 0.005 & 0.006 \\ 0.003 & 0.988 & -0.016 \\ -0.008 & -0.016 & 1.016 \end{vmatrix}$$

$t=0.60\times10^{-10}$ s

$$\begin{vmatrix} 1.016 & -0.065 & -0.052 \\ 0.036 & 1.016 & -0.031 \\ -0.006 & -0.060 & 1.001 \end{vmatrix}$$

$t=0.105\times10^{-9}$ s

$$\begin{vmatrix} 0.998 & -0.060 & -0.006 \\ 0.000 & 1.003 & -0.038 \\ 0.032 & -0.034 & 1.055 \end{vmatrix}$$

results were obtained by including intermolecular interactions in the equilibrium cell for this system. The average time in the simulation was on the order of 10^{-13} sec for this system, and the total number of time steps was 10^5. Also, the total number of molecular collisions with the fixed sphere was on the order of 10^4 collisions.

Alternatively and more comprehensively, the friction *tensor* can be determined through calculation of the force autocorrelation function from NNMD, Eq. (29) or Eq. (30). Table II gives a typical calculation for the values of $\zeta(t)/\zeta_{\text{anal}}$ under specular reflective boundary conditions for various times t and for the same parameters listed in Table I. As evident, the friction tensor is predicted to be diagonal (within experimental error) and independent of time. Note that each value listed is a mean value computed by repeating the "experiment" four times using different seeds for the random number generators; the results could be further improved running each simulation for a longer time. In any case, it is clear that the friction tensor is diagonal, isotropic, and independent of time as expected analytically. It is to be noted that the average velocity of the equilibrium-cell molecules, v_l ("free-stream" velocity), is taken to be zero for the force auto-

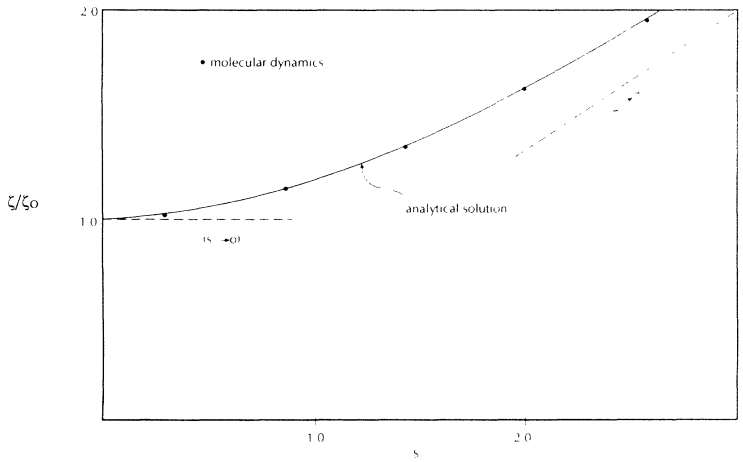

FIG. 3. Simulation results for free-molecule flow over a single spheres for small to large speed flows and specular reflective boundary conditions. Standard deviations are within a few percent or better of the mean values shown.

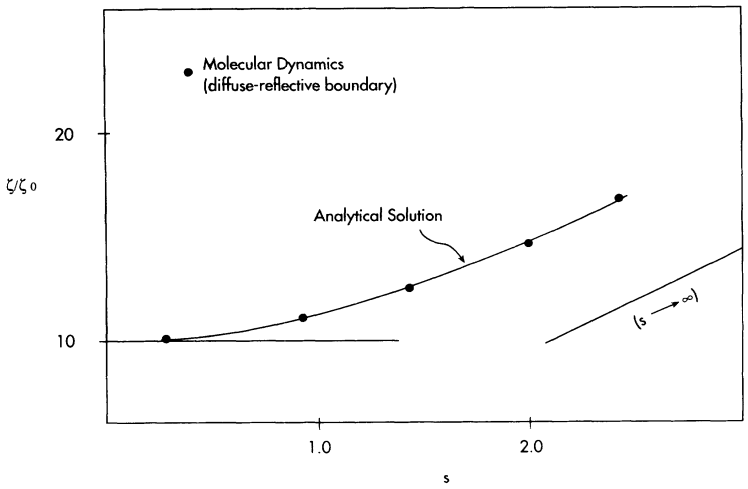

FIG. 4. Simulation results for free-molecule flow over a single spheres for small to large speed flows and diffuse reflective boundary conditions. Standard deviations are within a few percent or better of the mean values shown.

correlation calculations displayed in Table II as consistent with the basic theory underlying Eq. (29). For more discussion of the force autocorrelation function and Brownian motion theories in nonuniform systems, see [24]. Likewise, ζ_{anal} is taken from the low-speed result and is independent of v_l under these conditions.

More interestingly, a two-sphere system was selected for computational study that has only limited analytical results in the small Knudsen number gas region (see [25], and [26]) and no analytical results in the large Knudsen number, rarefied gas region. We note that this particular problem of many relatively massive spheres, with specular reflecting boundary conditions (scatterers) in a rarefied gas is dynamically the same as the so-called Lorentzian gas mixture [27].

In Fig. 5, calculated friction coefficients for two stationary equal-size spheres with free-stream gas velocity directed parallel to their line of centers is shown as a function of the intersphere separation distance. The remaining physical parameters are identical to those given previously for single spheres (Table I). Some interesting results are obtained in the two-sphere geometry including unequal friction coefficients and, hence, unequal aerodynamic forces exerted on the two spheres. In particular, the gas frictional force on sphere (1) is greatly reduced due to shielding by sphere (2). Thus, a relative or effective aerodynamic force exists in the two-sphere system that will cause the two spheres to coalesce, i.e.,

$$\mathbf{F}_{12}=\mathbf{F}_1-\mathbf{F}_2=v_z(\zeta_1-\zeta_2)\mathbf{e}_z \ . \tag{37}$$

Expressing this force in terms of a potential as

$$V_{12}(r)=v_z\int_r^{\infty}(\zeta_1-\zeta_2)dr' \ , \tag{38}$$

where $r=|\mathbf{r}_{12}|$ is the intersphere separation distance. The magnitude of this potential is shown to be quite large for the system of Fig. 5. In particular, it is estimated that $V_{12}(r=d)=300$ kT for this system. This behavior should be contrasted with the low-Reynolds-number continuum hydrodynamic behavior which predicts equal hydrodynamic forces on the two spheres (solid line in Fig. 5) and a symmetric two-particle friction tensor [10,28,29]. Small Knudsen number gas corrections to continuum

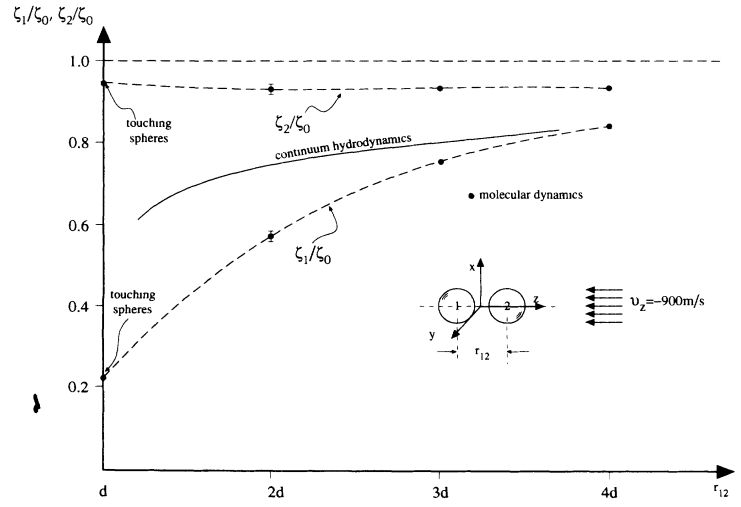

FIG. 5. Simulation results for free-molecule flows over two spheres as a function of the intersphere separation distance at relatively large free-stream velocities. The frictional force is, in general, less on the downstream sphere due to geometric shielding effects. Continuum hydrodynamics, and near continuum theories, predict parity of the frictional forces and a symmetric two-particle friction tensor. A typical standard deviation obtained for this system is shown for $r_{12}=2d$ (cf. Fig. 6).

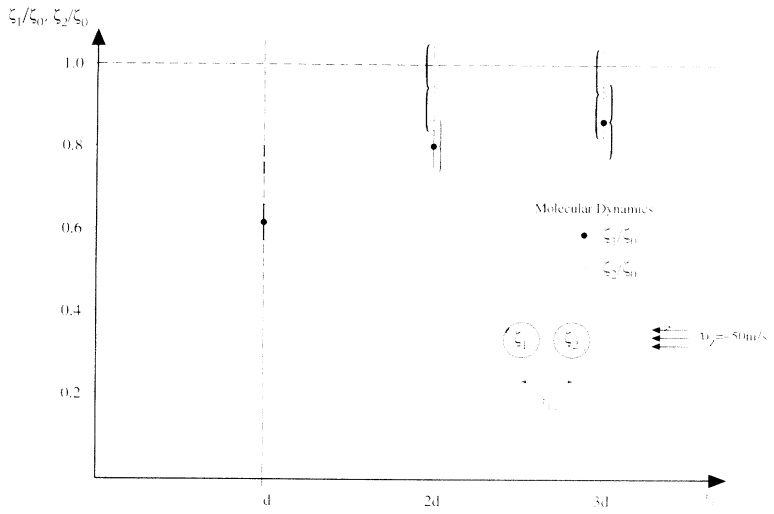

FIG. 6. Simulation results for free-molecule flows over two spheres as a function of intersphere separation distance at relatively small free-stream velocities. Here, again, the frictional force on the downstream sphere is less, although the differences are not as great as in Fig. 5 and only occur at small intersphere separations. Standard deviations in the time-average values can be reduced by running each simulation for a longer time.

behavior in the low-speed domain ($s \ll 1$) [25] also predict the equality.

An important result here is that the two-particle friction tensor for rarefied gas flows is not, in general, symmetric. This result is true for low-speed rarefied gas flows as well ($s \ll 1$) as shown in Fig. 6 and is a geometric "shielding" effect. For completeness, we also compared our results for touching spheres in parallel flow (Fig. 6) with those obtained by Chan and Dahneke [6]. In terms of a dimensionless drag coefficient c^*, as defined in Chan and Dahneke [6], we obtain $c^* = 13.66 \pm 1.14$ from the data in Fig. 6 (at $r_{12} = d$) as compared to $c^* = c_1^* + 4.59 \pm 0.04$ given by Chan and Dahneke [6], where c_1^* is the dimensionless drag coefficient for a single sphere and the variability of ± 0.04 is for the inner-half sphere calculations only. Using $c_1^* = 8\pi/3$ (see, e.g., [21]), the two mean values are seen to be in agreement within the standard deviations of the "experiments." Note that Chan and Dahneke [6] used a noise reduction scheme to reduce the variability of their results, and their technique was not employed here. As mentioned previously, the variability in the set of time-average values reported here (variance in the mean values) can be reduced by running each time-average value for a longer time in order to approach the true mean.

It is also interesting to note the effects of secondary molecular collisions in the two-sphere system, i.e., molecules that make more than one collision with object surfaces. In general, as expected, secondary collisions are more important at small intersphere separation distances and small free-stream gas velocities. More quantitatively, however, the ratio of secondary collisions to the total number of collisions is around 8% for touching spheres in Fig. 6 (low velocity case) and less than 1% for the $r_{12} = 3d$ case. These results suggest that a perturbation expansion in terms of a collision frequency parameter would appear to be a fruitful analytical approach for this system. In addition, secondary molecular collisions acting on the upstream sphere [sphere (2) in Figs. 5 and 6 tend to reduce its friction coefficient. Conversely, secondary collisions acting on the downstream sphere tend to increase its friction coefficient. The multicollisional effect is, however, of secondary importance to geometric shielding for this system.

Finally, we mention that the majority of the calculations reported here were obtained on a CRAY YMP computer with four CPU's. The average computational time for each data point, including variance determination shown in Fig. 5, for example, was 5000 seconds utilizing 2.7 megawords of memory.

V. CONCLUSIONS AND SUMMARY

A nonequilibrium molecular dynamics method has been developed and utilized for the study of free molecule, rarefied gas flows in complex geometries. The MD method for self-collisionless gas flows is far less computationally prohibitive as compared to collisional flows allowing for a wide-range investigation of the overall system dynamics. The MD method is a real-time simulation that allows for the analysis of important dynamical features, including force autocorrelation functions for geometrically complex objects in gas flows. A system of N spheres in a rarefied gas was selected for study because of its practical importance and lack of dynamical information on its behavior. Computations of the friction coefficient and force autocorrelation function for single spheres, under both specular and diffuse gas molecular boundary conditions, were shown to compare favorably with analytical solutions in the free-molecule gas regime. Interesting computational results for two spheres showed a nonsymmetric two-sphere friction tensor that leads to an effective, attractive gas dynamic force acting between the two spheres. The nonsymmetric nature of the two-particle friction tensor can be traced to geometric shielding effects and could have important consequences in such omnipresent phenomena as the coagulation of aerosols, among many others. The current computational method also demonstrates some exciting possibilities of probing long-time particle dynamics in complex systems by coupling molecular dynamics with generalized Langevin equation theory. The method could include not

only complex geometries, but also other complicated phenomena such as unique gas-molecule-surface interaction effects, among others. These problems and systems are under current investigation.

ACKNOWLEDGMENTS

I thank the Supercomputer Computational Research Institute at Florida State University for providing computer time and facilities.

APPENDIX: VELOCITY DISTRIBUTION ADJUSTMENTS

The Maxwellian velocity distribution is defined according to

$$f_\infty(\mathbf{v}_i)=\left[\frac{m}{2\pi kT_\infty}\right]^{3/2} \times\exp\left\{-\frac{m}{2kT_\infty}[(v_{x_i}-v_x)^2+(v_{y_i}-v_y)^2 +(v_{z_i}-v_z)^2]\right\}.$$

The values of $\mathbf{v}_i$ can be determined from the above distribution by a variety of methods (see, e.g., [11]). Then, to ensure the correct linear momentum a quantity β_l is subtracted from each velocity v_{li} where,

$$\beta_l=\left[\frac{1}{N}\sum_{i=1}^{N} v_{li}^{\text{old}}\right]-v_l \quad (l=x,y,z)$$

and

$$v_{li}^{\text{new}}=v_{li}^{\text{old}}-\beta_l .$$

This ensures that the average linear velocity is v_l.

Next, a correction to the deviation velocities is made to ensure the proper kinetic energy. Let

$$v'_{li}=v_{li}-v_l$$

and

$$\gamma=\frac{\sum_{i=1}^{N}\frac{1}{2}m(\mathbf{v}'_i\cdot\mathbf{v}'_i)}{\frac{3}{2}NkT_\infty} .$$

Then

$$v_{li}{}'^{\text{new}}=\frac{v_{li}{}'^{\text{old}}}{\sqrt{\gamma}}$$

will ensure that the average kinetic energy is $(\frac{3}{2})kT_\infty$. Note that this latter adjustment, involving the deviation velocities, will not affect the previous linear velocity adjustment involving β_l.

[1] D. J. Evans and G. P. Morriss, Comput. Phys. Rep. **1**, 297 (1984).

[2] W. G. Hoover and W. T. Ashurst, in *Theoretical Chemistry, Advances and Perspectives,* edited by H. Eyring and D. Henderson (Academic, New York, 1975), Vol. I, p. 1.

[3] L. Hannon, G. C. Lie, and E. Clementi, J. Stat. Phys. **51**, 965 (1988).

[4] J. A. Given and E. Clementi, J. Chem. Phys. **90**, 7376 (1989).

[5] C. Cercignani, *Theory and Application of the Boltzmann Equation* (Elsevier, New York, 1975), p. 262.

[6] P. Chan and B. Dahnecke, J. Appl. Phys. **52**, 3106 (1981).

[7] G. A. Bird, *Molecular Gas Dynamics* (Oxford University Press, Oxford, 1976).

[8] D. W. Heerman, *Computer Simulation Methods in Theoretical Physics* (Springer-Verlag, New York, 1986).

[9] W. G. Hoover, *Computational Statistical Mechanics* (Elsevier, New York, 1991).

[10] J. Happel and H. Brenner, *Low Reynolds Number Hydrodynamics* (Martinus Nijjoff, Boston, 1986).

[11] P. Bratley, B. L. Fox, and L. E. Schrage, *A Guide to Simulation* (Springer-Verlag, New York, 1983).

[12] J. J. Erpenbeck and W. W. Wood, *Statistical Mechanics, Part B,* edited by B. Berne (Plenum, New York, 1977).

[13] J. Kushich and B. J. Berne, *Statistical Mechanics, Part B,* edited by B. Berne (Plenum, New York, 1977), p. 41.

[14] W. Van Megen and I. Snook, Chem. Phys. Lett. **35**, 399 (1975).

[15] J. Lebowitz and E. Rubin, Phys. Rev. **131**, 2381 (1963).

[16] J. Lebowitz and P. Resibois, Phys. Rev. **139**, A1101 (1965).

[17] R. M. Mazo, J. Stat. Phys. **1**, 89 (1969).

[18] D. L. Ermak and H. Buckholtz, J. Comput. Phys. **35**, 169 (1980).

[19] H. S. Chan and K. A. Dill, Phys. Today **46**(2), 24 (1993).

[20] R. I. Cukier and J. M. Deutch, Phys. Rev. **177**, 240 (1969).

[21] S. A. Schaaf, in *Fluid Dynamics II,* Handbuch der Physik, Gruppe 3, Band 8, Teil 2, edited by S. Flügge and C. Truesdell (Springer, Berlin, 1963), pp. 591–624.

[22] R. O. Barrachina, D. H. Fujii, and C. R. Garibotti, Phys. Lett. **109A**, 447 (1985).

[23] F. Schürrer and G. Kügerl, Phys. Fluids A **2**, 609 (1990).

[24] R. M. Mazo, J. Stat. Phys. **1**, 101 (1969).

[25] R. Ying and M. H. Peters, J. Fluid Mech. **207**, 353 (1989).

[26] M. H. Peters and R. Ying, J. Aerosol Sci. **14**, 418 (1991).

[27] W. Sung and G. Stell, J. Chem. Phys. **77**, 4636 (1982).

[28] D. Bedeaux, A. M. Albano, and P. Mazur, Physica **88A**, 574 (1977).

[29] L. D. Landau and E. M. Lifshitz, *Statistical Physics, Part I,* 3rd ed. (Pergamon Press, New York, 1980).